Thermochimica Acta 513 (2011) 112–118

Contents lists available at ScienceDirect

Thermochimica Acta

journal homepage: www.elsevier.com/locate/tca

Isomorphism and phase diagram of $Pb_5(PO_4)_3F$–$Pb_5(PO_4)_3Cl$ system

A.V. Knyazev*, N.G. Chernorukov, E.N. Bulanov

Nizhny Novgorod State University, Gagarin Prospekt 23/2, 603950 Nizhny Novgorod, Russia

ARTICLE INFO

Article history:
Received 30 August 2010
Received in revised form 9 November 2010
Accepted 13 November 2010
Available online 19 November 2010

Keywords:
Apatite
Phase transition
High-temperature X-ray diffraction
Phase diagram

ABSTRACT

Compounds of composition $Pb_5(PO_4)_3F_xCl_{1-x}$ ($0 \le x \le 1$), which are synthetic analogues of minerals pyromorphite, flourapatite, and endlichite, were synthesized for the first time by high-temperature solid phase reactions. X-ray diffraction and IR spectroscopy were used to determine the structure of the compounds and revealed complete miscibility in the solid phase of the $Pb_5(PO_4)_3F$–$Pb_5(PO_4)_3Cl$ binary system. Adiabatic reaction calorimetry was used to measure standard enthalpies of mixing and formation and show that the regular solutions model is applicable to the $Pb_5(PO_4)_3F$–$Pb_5(PO_4)_3Cl$ system. Differential thermal analysis in tandem with high-temperature X-ray diffraction were used to study the phase diagram and characterize phase transitions.

1. Introduction

Compounds with the general formula $M^{II}_5(A^VO_4)_3L$ (M^{II} = Ca, Sr, Ba, Cd, Pb; A^V = P, As, V, Mn, Cr; L = OH, F, Cl, Br, I) are subjects of geochemistry and biochemistry. Most of the individual compounds of the aforementioned general formula and their base solid solutions are known as natural minerals, such as apatite $Ca_5(PO_4)_3F$, hydroxyapatite $Ca_5(PO_4)_3OH$, pyromorphite $Pb_5(PO_4)_3Cl$, endlichite $Pb_5(PO_4)_3F_xCl_{1-x}$, and some others [1,2]. Therefore, both science and technology are interested in their complex exploration. This work offers the results of a physicochemical study of $Pb_5(PO_4)_3F$–$Pb_5(PO_4)_3Cl$ system by X-ray diffraction methods, including high temperature experiments; IR spectroscopy; differential thermal analysis; and reaction calorimetry.

These compounds are structurally built of discrete phosphate tetrahedra linked to one another by lead polyhedra, which form joint layers (Fig. 1). Apatite-type structures typically offer two crystallographic positions for cations differing in coordination number and local symmetry. The lead atoms occupying the first positions 4f form polyhedra shaped as three-capped trigonal prisms PbO_9 having symmetry C_3 whose columns run along the threefold axis. Coordination number of lead atoms occupying the second position depends on type of ligand L: CR = 7 when L = F (2a) (distorted pentagonal bipyramids PbO_6F), whereas CR = 8 when L = Cl (2b) (distorted two-capped trigonal prisms PbO_6Cl_2).

In consequence of differences of halogen positions chlorine atoms of pyromorphite structure are located between layers formed by PO_4 tetrahedra, whereas fluorine atoms of fluorpyromorphite structure occupies positions in layers [3].

2. Experimental

2.1. Sample

Samples of $Pb_5(PO_4)_3F_xCl_{1-x}$ solid solution was prepared by the solid-state reaction between lead(II) nitrate, lead(II) fluoride, lead(II) chloride, and ammonium hydrophosphate:

$$4.5Pb(NO_3)_2 + 0.5xPbF_2 + 0.5(1-x)PbCl_2 + 3(NH_4)_2HPO_4 \rightarrow Pb_5(PO_4)_3F_xCl_{1-x} + 9NO_2 + 2.25O_2 + 6NH_3 + 4.5H_2O$$

A reaction mixture of a set stoichiometry was placed in a porcelain crucible and calcined at 350 and then 700 °C for 10 h with dispersion in an agate mortar every 2 h.

2.2. Apparatus and measurement procedure

The phase individuality of synthesized compounds was monitored by X-ray diffraction. X-ray diffraction patterns were recorded on a XRD-6000 Shimadzu diffractometer (CuKα radiation, geometry θ–2θ) in the 2θ range from 10° to 120° with scan increment of 0.02°.

High-temperature X-ray diffraction experiments in the range from 298 to 1173 K were carried out on the same diffractometer with increments of 0.02° ranging from 10° to 60° using an HA-1001 Shimadzu attachment.

Polycrystalline infrared spectra were measured with an FTIR-8400S Shimadzu spectrophotometer in KBr suspension for the

* Corresponding author. Tel.: +7 831 465 62 06; fax: +7 831 434 50 56.
E-mail addresses: knav@uic.nnov.ru, knyazevav@gmail.com (A.V. Knyazev).

0040-6031/$ – see front matter © 2010 Elsevier B.V. All rights reserved.
doi:10.1016/j.tca.2010.11.020

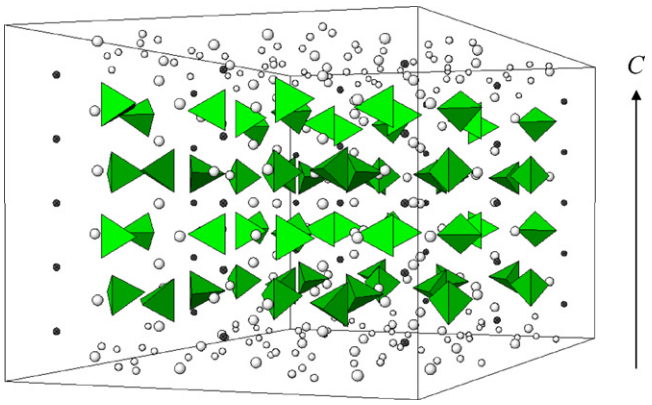

Fig. 1. Fragment of the $Pb_5(PO_4)_3Cl$ crystal structure.

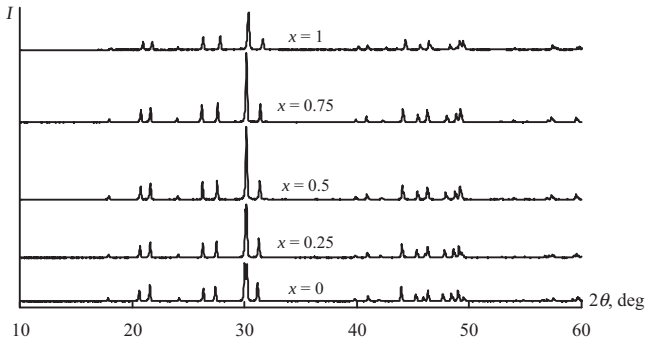

Fig. 2. X-ray diffraction patterns for $Pb_5(PO_4)_3F_xCl_{1-x}$.

4000–400 cm^{-1} region with resolution of 1 cm^{-1} and accumulation of 20 scan signals.

Thermal experiments were carried out on a LABSYS Setaram differential scanning calorimeter with a heating rate of 10 K/min. The experimental thermochemical data set was obtained using a modified Skuratov calorimeter. For the description and details of the experiment, see [4].

3. Results and discussion

3.1. X-ray diffraction

We synthesized solid solutions of compositions $Pb_5(PO_4)_3F_xCl_{1-x}$ (x = 0, 0.125, 0.25, 0.375, 0.5, 0.625, 0.75, 0.875, 1) using solid-phase reactions (Fig. 2). As follows from literature X-ray crystallography data for individual compounds $Pb_5(PO_4)_3F$ and $Pb_5(PO_4)_3Cl$ and from our powder diffraction studies solid solutions based on them, the $Pb_5(PO_4)_3F$–$Pb_5(PO_4)_3Cl$ system has complete solid miscibility, and unit cells of the compounds in question have hexagonal symmetry of space group $P6_3/m$ (Table 1). Analysis of variations in unit cell parameters as a function of composition allows us to infer that the Vegard rule holds in this system (Fig. 3).

Table 1
Unit cell parameters for compounds with the general formula $Pb_5(PO_4)_3F_xCl_{1-x}$.

x	a (Å)	c (Å)	V (Å)^3
0.00	9.940(1)	7.360(1)	629.7(1)
0.25	9.905(1)	7.381(1)	627.2(1)
0.50	9.880(1)	7.395(1)	625.1(1)
0.75	9.862(1)	7.408(1)	624.0(1)
1.00	9.799(2)	7.398(3)	615.1(1)

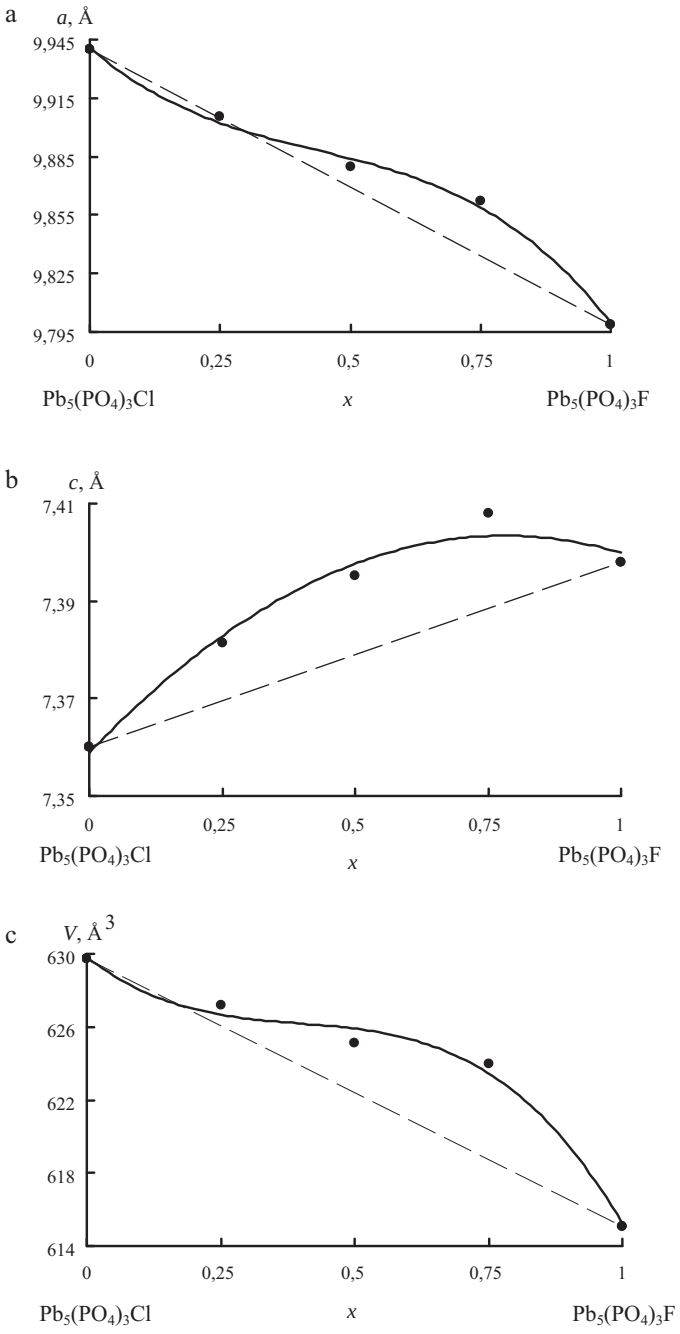

Fig. 3. Unit cell parameters and unit cell volume vs. composition of the solid solution.

There are positive deviations from Vegard and Retgers rules for all unit cell parameters. This fact demonstrates that individual compounds have stronger bonds in comparison with solid solutions in observable system.

There are two fields of solid solution composition in $Pb_5(PO_4)_3F$–$Pb_5(PO_4)_3Cl$ system: hypothetically solid solutions with $0 < x < 0.5$ are isostructural to pyromorphite, solid solutions with $0.5 \leq x < 1$ are isostructural to fluorpyromorphite. It should be noted that in second field bigger deviation of unit cell parameters from linear dependence was observed. Furthermore it is quite explainable that unit cell parameter a decreases when molar percent of less anion F increases. Anomalous growth of unit cell parameter c is the result of changing of halogen position in apatite structure.

Table 2
Band assignment in the IR spectra of compounds with the general formula $Pb_5(PO_4)_3F_xCl_{1-x}$ (cm^{-1}).

Assignment	0.00	0.25	0.50	0.75	1.00
ν (PO_4)	1031.9 s	1031.9 s	1030.0 s	1030.0 s	1026.1 s
	981.8 s	981.8 s	981.8 s	981.8 s	
	958.6 s	960.6 s	960.6 s	960.6 s	960.6 s
	922.0 w	922.0 w	922.0 w	922.0 w	922.0 w
δ (PO_4)	572.9 s	572.9 s	570.9 s	572.9 s	570.9 s
	540.1 s	538.1 s	538.1 s	542.0 s	540.1 s
	430.1 w	426.3 w	422.4 w	441.7 w	441.7 w

Notations: s—strong; w—weak.

3.2. IR spectroscopy

We carried out an IR spectroscopic study of the compounds in order to study their functional composition. In the IR spectra of the compounds of the general formula $Pb_5(PO_4)_3F_xCl_{1-x}$, two frequency ranges are distinguished (Table 2) where the vibrations of a phosphate tetrahedron appear. By the way of example, Fig. 4 shows IR spectra for individual compounds and a solid solution containing equimolar amounts of fluorine and chlorine. The stretching and bending vibrations of a phosphate tetrahedron appear in the ranges 1032–922 and 573–422 cm^{-1}, respectively.

Owing to the fact that differences between average bond distances of phosphate tetrahedra of pyromorphite and fluorpyromorphtie are not more than 1.8%, there are no sizeable changes of vibrational spectra in the range 1200–400 cm^{-1} during isomorphic substitution of fluorine for chlorine.

Further, in all test samples transparency in the IR range was discovered with a width of about 300 cm^{-1} over the wavenumber range of 1600–1200 cm^{-1} depending on the composition.

3.3. Thermochemistry

Calorimetric experiments were carried out in order to calculate standard enthalpies of formation and enthalpies of mixing and to elucidate the isomorphic miscibility model. For this purpose, we chose the thermochemical schemes below where 3 M nitric acid signed as a solvent.

Scheme 1 was used to determine the enthalpies of formation of $Pb_5(PO_4)_3F$ and $Pb_5(PO_4)_3Cl$. Reagent ratios were chosen so that the compositions of solutions 3 (3′) and 5 (5′) were identical. In view of this, the algebraic sum of equations (1.5·(1) + 0.5·(2) + (3)–(4)–(5)) for $Pb_5(PO_4)_3F$ and equations (1.5·(1) + 0.5·(2) + (3′)–(4′)–(5′)) for

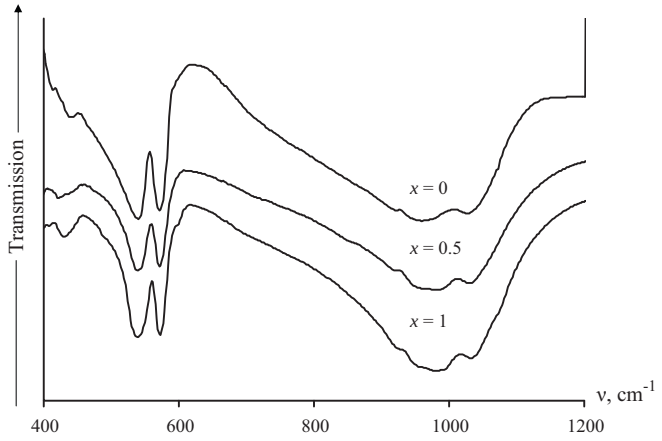

Fig. 4. IR spectra for compounds of composition $Pb_5(PO_4)_3Cl$, $Pb_5(PO_4)_3F_{0.5}Cl_{0.5}$ and $Pb_5(PO_4)_3F$.

Table 3
Enthalpies of solution and enthalpies of formation for the compounds used in thermochemical Scheme 1.

n	Compound	$\Delta_r H^\circ_n$ (kJ/mol)	$\Delta_f H^\circ$ (kJ/mol)
1	$Pb_3(PO_4)_2$ (cr)	−40.0 ± 0.2	−2426.0 ± 5.5 [5]
2	$Pb(NO_3)_2$ (cr)	4.7 ± 0.1	−451.7 ± 1.2 [6]
3	KF (cr)	−6.8 ± 0.4	−566.1 ± 1.3 [6]
3′	KCl (cr)	6.4 ± 0.3	−436.6 ± 0.3 [6]
5, 5′	KNO_3 (cr)	9.7 ± 0.1	−494.5 ± 0.5 [6]

$Pb_5(PO_4)_3Cl$ leads to Eqs. (6) and (6′), respectively:

$$\Delta_r H^\circ_6(298) = 1.5\Delta_r H^\circ_1(298) + 0.5\Delta_r H^\circ_2(298) + \Delta_r H^\circ_3(298) - \Delta_r H^\circ_4(298) - \Delta_r H^\circ_5(298)$$

$$\Delta_r H^\circ_6(298) = -17.6 \pm 0.8\ \text{kJ/mol}$$

$$\Delta_r H^\circ_{6'}(298) = 1.5\Delta_r H^\circ_1(298) + 0.5\Delta_r H^\circ_2(298) + \Delta_r H^\circ_{3'}(298) - \Delta_r H^\circ_{4'}(298) - \Delta_r H^\circ_{5'}(298)$$

$$\Delta_r H^\circ_{6'}(298) = 69.9 \pm 0.7\ \text{kJ/mol}$$

On the other hand, according to the Hess law,

$$\Delta_f H^\circ(298, Pb_5(PO_4)_3F, cr) = \Delta_r H^\circ_6(298) + 1.5\Delta_f H^\circ(298, Pb_3(PO_4)_2, cr) + 0.5\Delta_f H^\circ(298, Pb(NO_3)_2, cr) + \Delta_f H^\circ(298, KF, cr) - \Delta_f H^\circ(298, KNO_3, cr) \quad (10)$$

$$\Delta_f H^\circ(298, Pb_5(PO_4)_3Cl, cr) = \Delta_r H^\circ_{6'}(298) + 1.5\Delta_f H^\circ(298, Pb_3(PO_4)_2, cr) + 0.5\Delta_f H^\circ(298, Pb(NO_3)_2, cr) + \Delta_f H^\circ(298, KCl, cr) - \Delta_f H^\circ(298, KNO_3, cr) \quad (10')$$

These equations, together with the enthalpies of reactions (6) and (6′) and the standard enthalpies of formation of the reagents, were used to calculate the standard enthalpies of formation of the compounds at 298.15 K (Table 3).

Scheme 2 was used to determine the enthalpies of mixing and standard enthalpies of formation of solid solutions. Reagent ratios were chosen so that the compositions of solutions 1 and 2 were identical. In view of this, the algebraic sum of Eqs. (7) and (8) leads to Eq. (9), whose Hess enthalpy is

$$\Delta_r H^\circ_9(298) = \Delta_r H^\circ_7(298) - \Delta_r H^\circ_8(298) = \Delta_{mix} H^\circ(298) \quad (11)$$

According to [7], it is pertinent to refer the enthalpy of mixing to one mole of the atom to be substituted, and we indicate this in Eq. (11). Inspection of the resulting values shows that the enthalpy of mixing as a function of composition is fitted by a second-order polynomial (Fig. 5), in agreement with the regular solid solutions model:

$$\Delta_{mix} H^\circ(298)\,(\text{kJ/mol}) = 18.1 \cdot x_1 \cdot x_2 \quad (12)$$

Next, we found partial molar enthalpies of mixing using known thermodynamic relationships borrowed from [7]:

$$\Delta\overline{H_1} = 18.1 \times x_2^2 \qquad \Delta\overline{H_2} = 18.1 \times x_1^2 \quad (13)$$

The $\Delta_{mix} H^\circ$ (298) value and the enthalpies of formation of crystalline $Pb_5(PO_4)_3F$ and $Pb_5(PO_4)_3Cl$ were used to calculate the standard enthalpies of formation of solid solutions at 298.15 K (Table 4).

$Pb_3(PO_4)_2$ (cr) + HNO_3 (sln) → Solution 1 (1)

$Pb(NO_3)_2$ (cr) + Solution 1→ Solution 2 (2)

KF (cr) + Solution 2 → Solution 3 (3)

KCl (cr) + Solution 2 → Solution 3' (3')

$Pb_5(PO_4)_3F$ (cr, hex) + HNO_3 (sln) → Solution 4 (4)

$Pb_5(PO_4)_3Cl$ (cr, hex) + HNO_3 (sln) → Solution 4' (4')

KNO_3 (cr) + Solution 4(4') → Solution 5(5') (5,5')

1.5 $Pb_3(PO_4)_2$ (cr) + 0.5 $Pb(NO_3)_2$ (cr) + KF (cr) → $Pb_5(PO_4)_3F$ (cr, hex) + KNO_3 (cr) (6)

1.5 $Pb_3(PO_4)_2$ (cr) + 0.5 $Pb(NO_3)_2$ (cr) + KCl (cr) → $Pb_5(PO_4)_3Cl$ (cr, hex) + KNO_3 (cr) (6')

Scheme 1.

[$xPb_5(PO_4)_3F$ (cr, hex) + (1-x)$Pb_5(PO_4)_3Cl$ (cr, hex)] + HNO_3 (sln) → Solution 1 (7)

$Pb_5(PO_4)_3F_xCl_{1-x}$ (cr, hex) + HNO_3 (sln) → Solution 2 (8)

$xPb_5(PO_4)_3F$ (cr, hex) + (1-x)$Pb_5(PO_4)_3Cl$ (cr, hex) → $Pb_5(PO_4)_3F_xCl_{1-x}$ (cr, hex) (9)

Scheme 2.

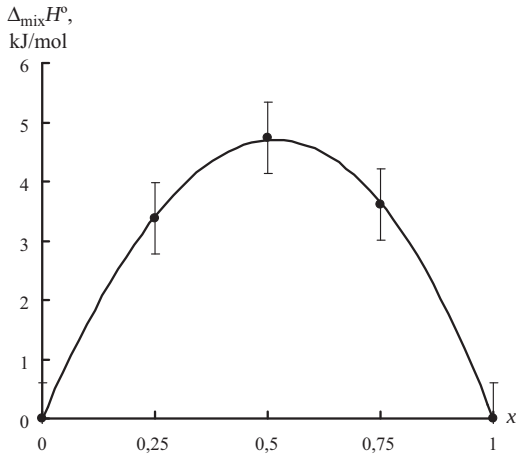

Fig. 5. Standard enthalpy of mixing vs. composition of the solid solution.

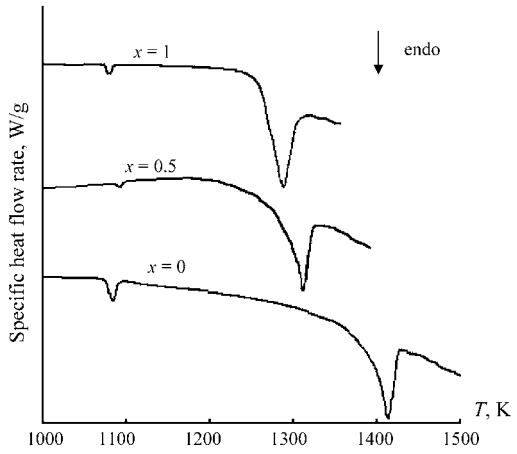

Fig. 6. Plot of the DTA-signal against temperature for $Pb_5(PO_4)_3F_xCl_{1-x}$.

3.4. Differential thermal analysis

Differential thermal analysis was used to determine phase-transition temperatures in the $Pb_5(PO_4)_3F$–$Pb_5(PO_4)_3Cl$ system. The DTA-curves feature two endotherms, one corresponding to the polymorphic transition and the other to melting (Fig. 6). Table 5 lists melting temperatures (T_{liq}), which correspond to points on the liquidus curves of the phase diagram, and polymorphic-transition temperatures (T_{tr}) for all compounds studied. The temperatures corresponding to points on the solidus curves (T_{sol}) were determined from exotherms on the DTA curves associated with crystallization of alloys during cooling [8,9].

3.5. High-temperature X-ray diffraction and phase diagram modeling

The phase-transition temperatures obtained in this way and the standard enthalpy of mixing as a function of composition were used for thermodynamic modeling of the $Pb_5(PO_4)_3F$–$Pb_5(PO_4)_3Cl$

Table 4
Standard enthalpies of solution in 3 M nitric acid, enthalpies of mixing, and enthalpies of formation (kJ/mol) for compounds with the general formula $Pb_5(PO_4)_3F_xCl_{1-x}$ (T = 298.15 K).

x	$\Delta_r H^\circ_{7}$	$\Delta_r H^\circ_{8\,(4,4')}$	$\Delta_{mix} H^\circ$	$\Delta_f H^\circ$
0	−131.0 ± 0.4	−131.0 ± 0.4	0	−3737 ± 8
0.25	−95.6 ± 0.4	−99.0 ± 0.4	3.4 ± 0.6	−3788 ± 9
0.5	−81.0 ± 0.4	−85.7 ± 0.4	4.7 ± 0.6	−3841 ± 10
0.75	−74.3 ± 0.4	−77.9 ± 0.4	3.6 ± 0.6	−3896 ± 11
1	−56.6 ± 0.5	−56.6 ± 0.5	0	−3954 ± 7

Table 5
Phase-transition temperatures in compounds with the general formula $Pb_5(PO_4)_3F_xCl_{1-x}$.

x	T_M (K)	T_{tr1} (K)	T_{tr2} (K)	T_{sol} (K)	T_{liq} (K)
0	–	1084	1084	1415	1415
0.25	723	1069	1093	1283	1347
0.5	823	1065	1092	1280	1312
0.75	773	1064	1087	1262	1284
1	–	1073	1073	1289	1289

Table 6
Thermal expansion coefficients vs. temperature for hexagonal modification of $Pb_5(PO_4)_3F$ and $Pb_5(PO_4)_3Cl$.

T (K)	a (Å)	α_a ($\times10^6$ K^{-1})	c (Å)	α_c ($\times10^6$ K^{-1})	V (Å)^3	α_V ($\times10^6$ K^{-1})
$Pb_5(PO_4)_3F$ (T_{tr} = 1073 K)						
298	9.843(2)	10.3	7.404(2)	10.3	621.3(3)	30.9
373	9.852(2)	11.6	7.413(2)	12.8	623.4(3)	35.9
473	9.865(2)	13.2	7.428(2)	16.2	626.0(2)	42.6
573	9.889(1)	14.8	7.439(1)	19.5	630.1(1)	49.2
673	9.897(1)	16.5	7.456(1)	22.9	632.4(1)	55.8
773	9.908(1)	18.1	7.472(1)	26.2	635.2(1)	62.4
873	9.926(1)	19.7	7.488(1)	29.5	638.8(1)	68.9
973	9.947(1)	21.3	7.516(1)	32.7	644.0(1)	75.3
1023	9.961(1)	22.1	7.529(1)	34.3	647.0(2)	78.6
1073	9.980(2)	22.9	7.546(2)	35.9	651.0(2)	81.8
$Pb_5(PO_4)_3Cl$ (T_{tr} = 1084 K)						
298	9.9538(9)	1.5	7.3693(9)	12.1	632.3(1)	15.1
373	9.9624(9)		7.3772(9)	14.0	634.1(1)	17.0
473	9.9770(7)		7.3866(7)	16.5	636.7(1)	19.5
573	9.9898(9)		7.4017(9)	19.0	639.7(1)	22.0
673	10.0067(9)		7.416(1)	21.5	643.1(1)	24.5
773	10.022(1)		7.434(1)	24.0	646.6(1)	27.0
873	10.039(1)		7.450(1)	26.4	650.2(1)	29.5
973	10.0532(8)		7.4721(9)	28.9	654.0(1)	31.9
1073	10.069(1)		7.495(1)	31.3	658.1(1)	34.3

phase diagram, this modeling comprising the steps of: (1) calculating the solid solution decomposition temperatures (T_M), i.e., the Becker curve; (2) determining the polymorphic transition temperature as a function of composition; and (3) calculating solidus and liquidus temperatures based on crystal–liquid equilibrium.

Temperatures on the Becker curves (Table 5) were found from the relationship $T_M = \Delta_{mix}H^\circ/\Delta_{mix}S^\circ$ [10]. The standard enthalpy of mixing was set equal to the configurational entropy and calculated from $\Delta_{mix}S^\circ(298) = -R(x_1 \ln x_1 + x_2 \ln x_2)$.

The variation in the reversible polymorphic transition temperature is fitted by a second-order polynomial:

$$T_{tr1} = 58.9x^2 - 69.1x + 1083.7$$

$$T_{tr2} = -57.1x^2 + 45.9x + 1084.3$$

We carried out high-temperature X-ray diffraction experiments to elucidate structural alterations accompanying the transition. For both $Pb_5(PO_4)_3F$ and $Pb_5(PO_4)_3Cl$, we found that the polymorphic transition lowers the unit cell symmetry from hexagonal (space group $P6_3/m$) to monoclinic (space group $P112_1/b$). At T_{tr}, there is a discontinuity on the unit cell parameter and unit cell volume plots (Fig. 7).

High-temperature X-ray diffraction was used not only for studying phase transitions, but also for determining thermal expansion coefficients (Tables 6 and 7). For solving this problem, $a = f(T)$ equations were fitted by linear and quadratic functions and calculations were carried out in DTC program [11].

The data compiled in Table 6 show that $Pb_5(PO_4)_3F$ and $Pb_5(PO_4)_3Cl$ crystals, regardless of the polymorph, have a considerable anisotropy of thermal expansion, and this phase of the apatite family may be classified as a strongly expanding compound in terms of the classification system described in [12].

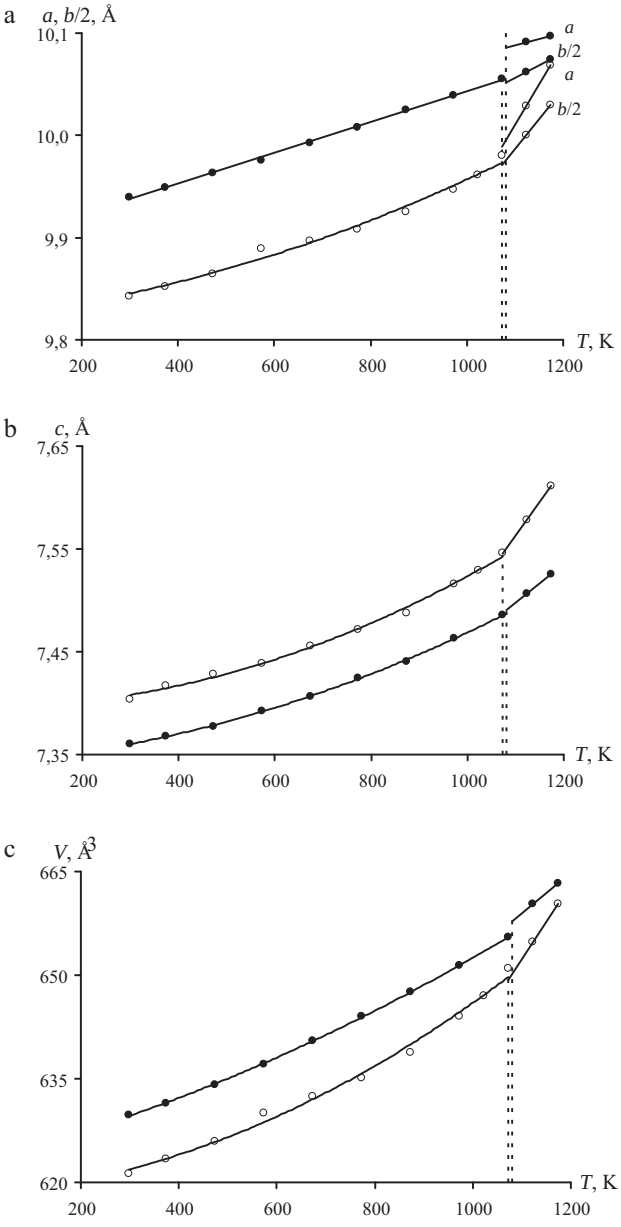

Fig. 7. Unit cell parameters and unit cell volume vs. temperature for $Pb_5(PO_4)_3F$ (white circles) and $Pb_5(PO_4)_3Cl$ (black circles).

As can be seen from Table 6 thermal expansion coefficient along crystallographic axis a for $Pb_5(PO_4)_3F$ is tenfold more than in $Pb_5(PO_4)_3Cl$, that connected with location in layer of F atoms.

Volume thermal expansion coefficients of monoclinic modifications phases under study in field of polymorphic transition increase twice or thrice in comparison with similar coefficients of hexagonal modifications.

Table 7
Thermal expansion coefficients vs. temperature for monoclinic modification of $Pb_5(PO_4)_3F$ and $Pb_5(PO_4)_3Cl$.

T (K)	a (Å)	α_a ($\times10^6$ K^{-1})	b (Å)	α_b ($\times10^6$ K^{-1})	c (Å)	α_c ($\times10^6$ K^{-1})	γ (°)	α_γ ($\times10^6$ K^{-1})	V (Å)^3	α_V ($\times10^6$ K^{-1})
$Pb_5(PO_4)_3F$ (T_m = 1289 K)										
1123	10.029(2)	79.8	20.000(3)	39.0	7.578(2)	86.9	120.48(2)	33.2	1309.7(3)	165.0
1173	10.069(2)		20.039(4)		7.611(2)		120.68(2)		1320.8(3)	
$Pb_5(PO_4)_3Cl$ (T_m = 1415 K)										
1123	10.105(2)	11.9	20.151(3)	24.8	7.516(2)	50.6	119.96(2)	0	1325.8(3)	87.2
1173	10.111(2)		20.176(2)		7.535(2)		119.96(1)		1331.8(3)	

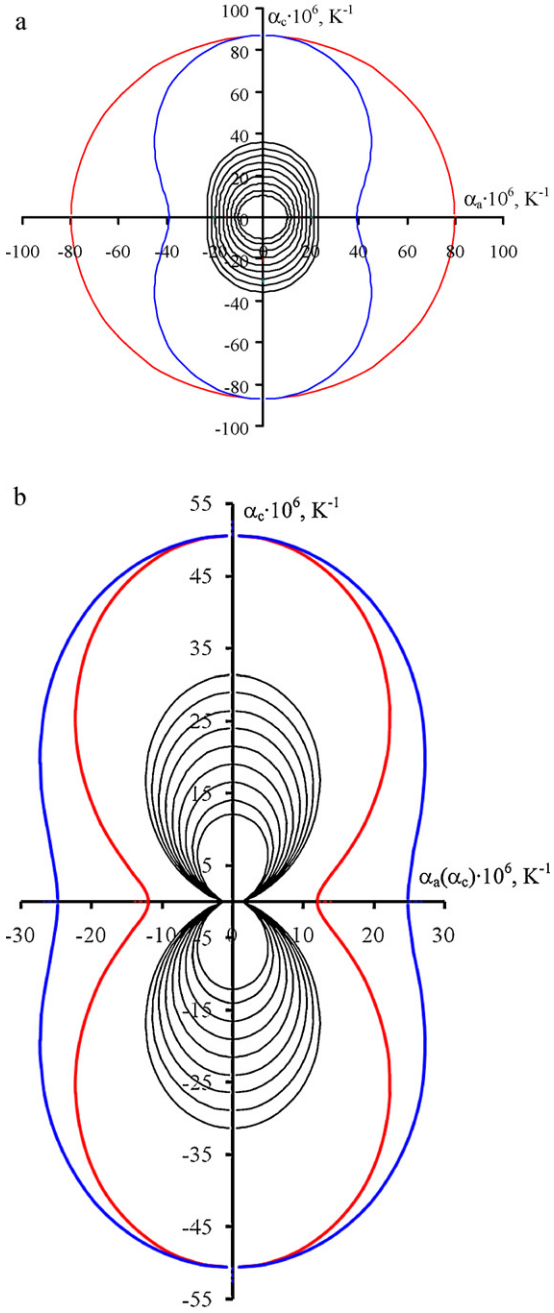

Fig. 8. Thermal expansion diagrams for $Pb_5(PO_4)_3F$ (a) and $Pb_5(PO_4)_3Cl$ (b) at crystallographic plane *ac* for hexagonal modification (black line) and at crystallographic plane *ac* (red line) and *bc* (blue line) for monoclinic modification.(For interpretation of the references to color in this figure legend, the reader is referred to the web version of the article.)

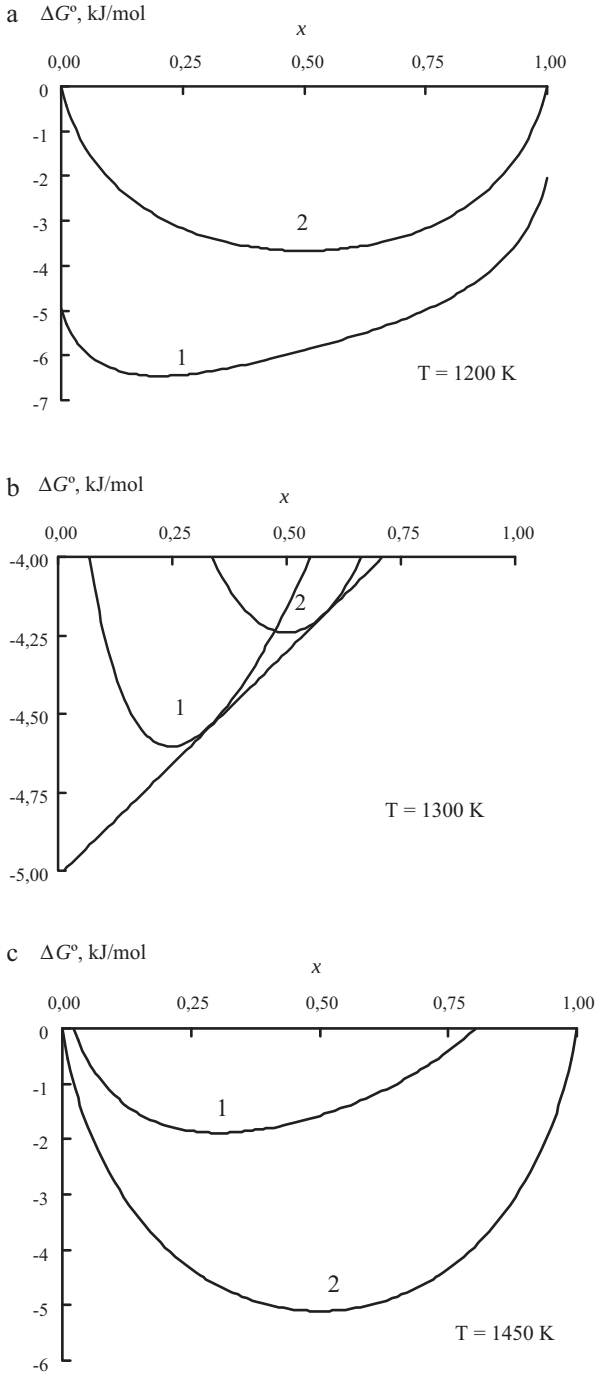

Fig. 9. Standard Gibbs function vs. composition of (1) crystal and (2) liquid at various temperatures.

It is significant that monoclinic modification is pseudohexagonal and polymorphic transition can be described as collapse transition in terms of Burgers classification [7]. Also that transition is reversible. Crystallographic axes *c* are equivalent in both polymorphic modifications. Thereof that $\gamma \neq 120^\circ$ crystallographic axes *a* and *b* of monoclinic modification some differ from crystallographic axes in hexagonal modification.

Fig. 8 shows thermal expansion diagrams for $Pb_5(PO_4)_3F$ and $Pb_5(PO_4)_3Cl$ at different crystallographic planes. Value of thermal expansion coefficient in given direction corresponds to length of radius-vector which is traced from origin of coordinates to edge of figure of expansion. To construct thermal expansion diagram at the given temperature values of thermal expansion coefficients along two crystallographic axes at the same temperature are inputted to KTP program (on this occasion it was axes *a*–*c* for hexagonal modifications of compounds under study; *a*–*c* and *b*–*c* for monoclinic modification) [11]. Diagrams at different temperatures are plotted on the same coordinate plane to get more illustrative example of thermal expansion dynamics.

In spite of structural alterations, the preferred crystallographic direction upon expansion is the unit cell parameter *c*, which is due to the greater strength of chemical bonds in layers formed by PO_4 tetrahedra compared to interlayer interactions.

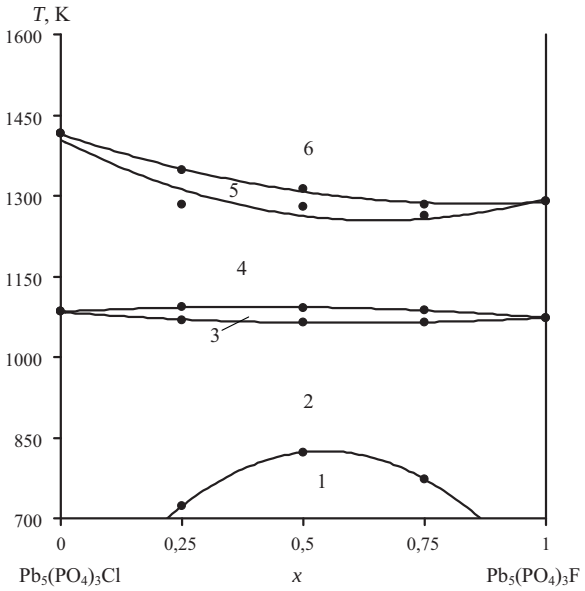

Fig. 10. $Pb_5(PO_4)_3F$–$Pb_5(PO_4)_3Cl$ phase diagram. Notations: (1) mixture of solid solutions, (2) solid solution (the hexagonal phase), (3) mixture of two phases of solid solutions, (4) solid solution (the monoclinic phase), (5) solid solution (monoclinic phase) + liquid, and (6) liquid.

In calculating solidus and liquidus temperatures, we used the general form of the Clausius–Clapeyron equation:

$$\ln \frac{x_l \cdot \gamma_l}{x_c \cdot \gamma_c} = -\frac{\Delta_{fus} H^\circ}{R} \left(\frac{1}{T} - \frac{1}{T_{liq}} \right) \quad (14)$$

because regular liquid and solid solutions are characteristic of the $Pb_5(PO_4)_3F$–$Pb_5(PO_4)_3Cl$ system, as shown by thermochemical studies. Eq. (14) for a binary system may be represented by the set

$$\begin{aligned} \ln x_{\ell,1} + \frac{\Omega_\ell \cdot (1 - x_{\ell,1})^2}{RT} - \ln x_{c,1} - \frac{\Omega_c (1 - x_{c,1})^2}{RT} &= -\frac{\Delta_{fus,1} H^\circ}{R} \left(\frac{1}{T} - \frac{1}{T_{liq,1}} \right) \\ \ln x_{\ell,2} + \frac{\Omega_\ell \cdot (1 - x_{\ell,2})^2}{RT} - \ln x_{c,2} - \frac{\Omega_c (1 - x_{c,2})^2}{RT} &= -\frac{\Delta_{fus,2} H^\circ}{R} \left(\frac{1}{T} - \frac{1}{T_{liq,2}} \right) \end{aligned} \quad (15)$$

Set (15) was used to calculate the thermodynamic parameters of the liquid (Ω_l = 13000 J) and the crystal (Ω_c = 18100 J) and the enthalpies of melting of the first component and the second component ($\Delta_{fus,1} H^\circ$ = 32545 J/mol and $\Delta_{fus,2} H^\circ$ = 29647 J/mol, respectively). This solved the inverse problem; that is, simulation was based on experimentally derived data on phase boundaries [13]. The values obtained in this way were used to construct the plots of the Gibbs energies versus composition for a liquid and a crystal (Fig. 9) and the phase diagram (Fig. 10). Fig. 7 gives three examples of $\Delta G = f(X)$: in the first example (T = 1250 K), thermodynamic stability is characteristic of the crystal; in the second (T = 1300 K), of crystal + liquid; and in the third (T = 1450 K), of the liquid. The upper portion of the diagram (Fig. 8) is shaped as a distorted lens, the shape corresponding to a system with insignificant nonidealities in liquid and solid solutions where components are completely miscible.

A comparison of $Pb_5(PO_4)_3Cl$–$Pb_5(VO_4)_3Cl$ phase diagram [5] with concerned phase diagram enables to make a conclusion that $Pb_5(PO_4)_3F$–$Pb_5(PO_4)_3Cl$ system has greater deviation from ideality than in Ref. [5]. Greater curvature of solidus and liquidus curves and greater value of mixture enthalpy are evidences of that. These facts confirm complicated character of isomorphic substitutions which is accompanied by changing of crystallographic positions in comparison with classic isomorphic substitution in $Pb_5(PO_4)_3Cl$–$Pb_5(VO_4)_3Cl$ system.

In summary, we have studied the $Pb_5(PO_4)_3F$–$Pb_5(PO_4)_3Cl$ system using X-ray diffraction, IR spectroscopy, differential thermal analysis, and calorimetry and constructed a phase diagram for this system.

References

[1] A. G. Betekhtin, The Course of Mineralogy, Gosudarstvennoe izdatel'stvo geologicheskoi literatury, Moscow, 1951, [in Russian].
[2] G.N. Vertushkov, V.N. Avdonin, Tables for Mineral Determination Based on Chemical and Physical Properties: A Handbook, Nedra, Moscow, 1992 [in Russian].
[3] Y. Dai, J.M. Hughes, Can. Mineral. CAMIA 27 (189) (1989).
[4] S.M. Skuratov, V.P. Kolesov, A.F. Vorob'ev, Thermochemistry, vol. 2, Mosk. Gos. Univ., Moscow, 1966 [in Russian].
[5] N.G. Chernorukov, A.V. Knyazev, E.N. Bulanov, Zhurnal Neorganicheskoi Khimii 55 (1549) (2010).
[6] V.P. Glushko (Ed.), The Thermal Constants of Materials, Issues I–X, Nauka, Moscow, 1968-1981 [in Russian].
[7] V.S. Urusov, Theoretical Crystal Chemistry, Mosk. Gos. Univ., Moscow, 1987 [in Russian].
[8] D. Klimm, I.M. Ranieri, R. Bertram, S. Baldochi, Mater. Res. Bull. 43 (676) (2008).
[9] D. Yimin, W. Ping, L. Xu, Zh. Tingting, Thermochim. Acta 472 (38) (2008).
[10] R. Becker, Z. Metallkunde 29, 8 (1937).
[11] R.I. Belousov, S.K. Filatov, Glass Phys. Chem. 33 (377) (2007).
[12] S.K. Filatov, High-Temperature Crystal Chemistry. Theory, Methods, and Results, Nedra, Leningrad, 1990 [in Russian].
[13] K. Lyupis, Chemical Thermodynamics of Materials, Metallurgiya, Moscow, 1989 [in Russian].